Jurnal Kejuruteraan 38(1) 2026: 399-411
https://doi.org/10.17576/jkukm-2026-38(1)-35

Membrane Fouling and Flux Reduction of *Nannochloropsis Sp* Protein Hydrolysate using Cross-Flow Ultrafiltration Membrane

Nur Izzati Md Saleh[a], Wan Azlina Wan Ab Karim Ghani[a*], Siti Mazlina Mustapa Kamal[b], Azil Bahari Alias[c] & Mohd Razif Harun[a]

[a]*Sustainable Process Engineering Research Centre (SPERC),*
Faculty of Engineering, Universiti Putra Malaysia, Malaysia 43400 UPM, Serdang, Selangor, Malaysia

[b]*Department of Food & Process Engineering,*
Faculty of Engineering, Universiti Putra Malaysia, Malaysia 43400 UPM, Serdang, Selangor, Malaysia

[c]*Industrial Process Reliability and Sustainability (INPRES), Faculty of Chemical Engineering,*
Universiti Technologi MARA, 40450 Shah Alam, Selangor, Malaysia

[*]*Corresponding author: wanazlina@upm.edu.my*

Received 14 May 2024, Received in revised form 3 September 2025
Accepted 3 October 2025, Available online 30 January 2026

ABSTRACT

Microalgae protein hydrolysate enriched in peptide was produced by the enzymatic hydrolysis of Nannochloropsis sp. To obtain smaller peptides fractions, an ultrafiltration membrane was used to fractionate the hydrolysate, which contained a wide range of peptide sizes. However, a significant limitation of ultrafiltration membranes is flux reduction time due to fouling. This study investigates the influence of operational parameters variables such as flow rate, transmembrane pressure and pH on flux reduction and membrane fouling behaviour. Three membrane configurations (10 kDa, 5 kDa and two-stage 10/5 kDa) were evaluated. Kumar's pore-blocking models were applied to the optimal configuration with the largest permeate flux to analyse fouling mechanism. The results showed that permeate flux was declined over time and stabilized within 20 to 35 minutes under all conditions. The best performance for microalgae protein hydrolysate fractionation was observed with two-stage 10/5 kDa membrane at a flow rate of 23 ml/min, TMP of 1.5 bar, and pH 2. The standard pore-blocking model effectively predicted the flux reduction, confirming the role of membrane fouling in performance decline. This study highlights that optimizing ultrafiltration membrane parameters and selecting the appropriate membrane configuration can mitigate fouling effects, enhancing flux stability and peptide transmission.

Keywords: Microalgae protein hydrolysate; membrane fouling; flux reduction; ultrafiltration membrane; pore blocking model

INTRODUCTION

Nannochloropsis sp is type of microalgae having oleaginous properties and high concentration of eicosapentaenoic acid (EPA). In Malaysia, microalgae *Nannnochloropis sp* is widely used in the aquaculture industry as a feed (Abidin et al.2020). It is also known as a potential source of larva feed and biofuel production due to its high triacylglycerol (TAG) content (up to 60% of its dry weight) (Gouveia & Oliveira, 2009). Due to the high cost of producing biofuel, most studies focused on the idea of a microalgae biorefinery, in which the entire biomass of the algae is used: both the primary product (oil) and byproducts (protein, carbohydrates and fiber). Other than lipids, protein is one of the highest contents in microalgae, up to 50% w/w which has a value added (Medina et al. 2015). Peptides derived from microalgae protein's *Nannochloropsis sp* have promising wide biological activities (Nguyen et al. 2013; Qian et al. 2013; Samarakoon et al. 2013). Enzymatic hydrolysis is the most preferred method in the production of peptides because it has high specificity for peptide bond-cleaving and consistent product properties (Aluko, 2018). However, *Nannochloropsis sp* microalgae protein hydrolysate (MPH) contains a wide

range of functional peptides sizes in a large number of hydrolyzed protein fractions (Bazinet & Firdaous 2009). More powerful antioxidative peptides have been found in smaller peptide sizes (Fan et al. 2012).

Numerous studies conducted over the past 20 years have demonstrated the feasibility of fractionating peptide from protein hydrolysate using ultrafiltration, with the majority of them have focused on the role of operating parameters on permeate flux decrease (Vela et al. 2008; Md Zain & Mohammad 2016). The main challenge in assessing whether the ultrafiltration membrane process will be effective is fouling. The fouling phenomena could be due to the concentration polarization, formation of a cake layer or membrane pore blocking (Koonani & Amirinejad 2019). This effect could be mitigated by using appropriate operating parameters, membrane pore size and design. However, limited studies have been undertaken on the fouling analysis of protein hydrolysate and the influence of process parameters on fouling especially from microalgae. According to Vela et al. (2008), membrane filtration assessments were performed under various experimental conditions to obtain data on permeate flux variation with time. Despite some progress in the fundamental fouling mechanisms of ultrafiltration membranes, further research is required to fully understand the fouling mechanisms.

There are many empirical models in the literature, but there are also several semi-empirical models to be discovered (Vela et al. 2008). Finally, empirical models are quite accurate, but it is not possible to fully characterize the fouling mechanisms that occur during membrane filtration. Completely theoretical models can aid in understanding the fouling phenomena. Fortunately, those reported in the literature failed to anticipate accurately the declination of permeate flux in ultrafiltration without the utilization of experimental data to determine some model parameters. Hence, semi-empirical models with physical clear parameters offer a reliable alternative for accurately estimation the declining trend of permeate flux throughout ultrafiltration whilst elucidating fouling mechanisms (Vela et al. 2008).

In this study, Kumar's semi-empirical models that describe the permeate flux decline for cross-flow ultrafiltration presented by Kumar's model (cake layer formation, standard pore blocking, and complete pore plugging) were utilized to comprehend the fouling mechanism under various operating conditions. A model fitting can be performed to determine the correlations between experimental and predicted data using Kumar's linearized equation. By using a fitting model, better understanding of the factors that influence fouling and the type of fouling that predominate. Meanwhile, to gather information on permeate flux variations over time, this study investigated operating parameters such as flow rate, transmembrane pressure and pH at various membrane pore sizes.

METHODOLOGY

PREPARATION OF MICROALGAE PROTEIN HYDROLYSATE

Nannochloropsis sp microalgae protein hydrolysate (MPH) was produced by hydrolysis with Alcalase enzyme from Bacillus licheniformis Subtilisin A strain with 2.4 activity units AU/g. The reaction catalyzed by Alcalase was performed at 50°C, pH 8, 100 mL of 50 mM phosphate buffer solution, enzyme concentration of 0.3 g/L and substrate concentration of 5 g/L, reaction time of 24 hours and shaking speed of 80 rpm. Following the reaction, the hydrolysis was terminated by heating the mixture in a water bath at 95°C for 10 minutes. The mixture was allowed to cool before being centrifuged at 4000 g (centrifuge model KUBOTA) for 20 minutes and then filtered. The microalgae residue was removed and the supernatant MPH was collected for the fractionation process.

EXPERIMENT EQUIPMENT

An ultrafiltration membrane (QuixStand- Benchtop system) was used for MPH fractionation. A hollow fiber cross flow filtration cartridge made by GE healthcare was used in the The QuixStand benchtop system. A 400 mL feed reservoir, lower and upper manifolds, a support rod, and an entrance and outlet pressure gauges were all part of the system. The process solution is kept in the reservoir, which also collects the retentate stream and supplies it to the recirculation pump. The sanitary connector on the lower manifold was linked to the feed reservoir. The system consists of reservoir cover, gasket, and clamp. The cap includes two barbed inlet ports that link the tube to the cap. The wo ports on the cap enabled for the retentate stream to be recirculated back to the reservoir, as well as the recirculation of additional feed solution or diafiltrate during processing. Two distinct hollow fiber membrane cartridges sizes with surface area of 140 cm^2 and a molecular weight cut-off (MWCO) of 5 and 10 kDa (Xampler Cartridge, GE Healthcare Bio-Science, Westborough, USA) were utilised in this investigation. The cartridges were made of polysulfone (PS) materials. Both UF membrane cartridges were operated vertically for better drainage and higher recovery.

As shown in Figure 1, a single crossflow UF membrane with 10 kDa and 5 kDa membranes were utilized independently throughout the operation. Meanwhile, with

two-stage cross flow UF membrane, a 10 kDa membrane cartridge was used during first filtration, and the permeate was used as a feed at second filtration, which used 5 kDa membrane cartridge, as shown in Figure 2.

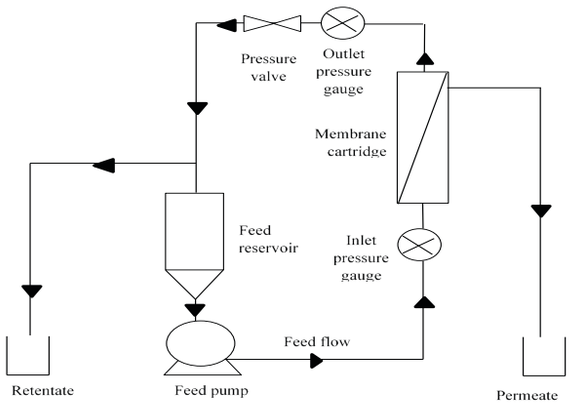

FIGURE 1. Schematic diagram of single cross flow UF membrane

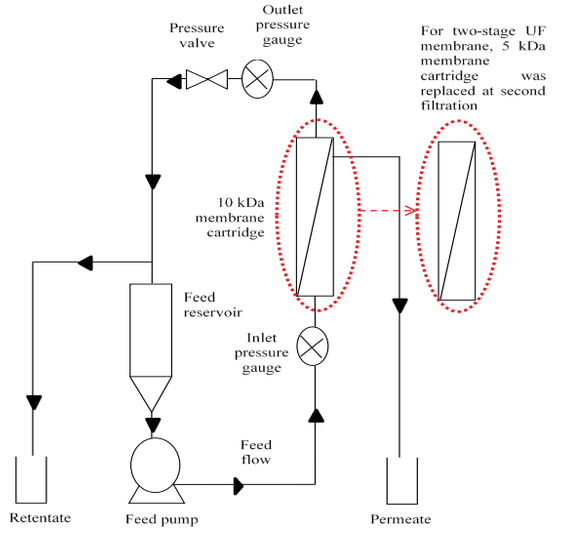

FIGURE 2. Schematic diagram of two-stage cross-flow UF membrane

FRACTIONATION PROCESS OF MICROALGAE PROTEIN HYDROLYSATE

The fractionation process of MPH was assessed using a cross-flow ultrafiltration membrane system with two different configurations; a single and two-stage membrane. In fractionated MPH, the performance of single membranes (10 kDa and 5 kDa) and two-stage membrane (10/5 kDa) were investigated. In addition to the configuration membrane, the pH, flow rate and transmembrane pressure were also evaluated. The selection of these parameters was based on combination of preliminary experiments and literature studies (add references). The flow rate of 23, 39, 35 and 41 ml/min was varied and adjusted using a peristaltic pump. The selected flow rate was chosen to balance permeate flux enhancement and minimized membrane fouling which is consistent with Liu et al, 2020 that reported that optimal flow rates in the range of 20–30 mL/min for similar molecular weight cut-off (MWCO) (Liu et al. 2020). Transmembrane pressure of 0.5, 1.0 and 1.5 bar, with a constant flow rate of 23 ml/min controlled by the back-pressure valve, were also investigated. Studies shown that for UF membranes with MWCO between 5-10 kDa, an optimal range of 1.0-1.5 bar achieves good separation while minimizing irreversible fouling (Chen et al, 2021). The pH effect (pH 2, pH 4, pH 7 and pH 9) was studied by altering acidity with 1.0 N of hydrochloric acid, (HCl) and alkalinity using 1.0 N of sodium hydroxide (NaOH). The feed flow rate was manually selected manually after running the UF membrane in an open system with deionized water at speeds 100 (minimum), 200, 300 and 400 rpm (maximum). The feed flow rate is determined by calculating the volume of permeate over time. Ranges for transmembrane pressure were also chosen based on the limitation of the membrane system setup, which allows for a maximum transmembrane pressure of 1.5 Bar. The selection of range for pH was discussed by Roslan et al. (2017) and Wang et al. (2019) which suggested that pH adjustments away from isoelectric point (pI) improve flux and reduce fouling. The fractionation process took 35 minutes per run, with the volume of permeate collected every 5 minutes. The fractionation time was determined as the feed entered the membrane cartridge. The experimental data were utilized to assess the UF membrane's performance based on their permeate flux.

PERMEATE FLUX

The permeate flux was measured at specified intervals every 5 minutes to assure accuracy t (Wang & Tang, 2011). Permeate flux, J (L/m2,h) was calculated according using equation (1) by (Zain et al. 2017).

$$\text{Flux, } J = \frac{V}{At} \quad (1)$$

Where V is the volume of permeate collected (L), A is membrane surface area (m^2) and t is filtration time (h).

PEPTIDE TRANSMISSION

The peptide transmission of MPH was analysed based on size distribution using AKTA Fast Pressure Liquid

Chromatography (FPLC, Amersham Pharmacia Biotech) equipped with sensor at wavelength 280 nm. The sample was fractionated using a prepacked Tricorn™ glass column (Superdeck™30 Increase 10/300 GL) in which the matrix was built from the composite of cross-linked agarose and dextran. Prior analysis, deionized water and two buffers were prepared; 20% ethanol and 0.05 Mtris-HCL buffer at pH 7. All the buffers and deionized water were prepared for 1L, sonicated for 20 minutes using water bath sonicator (1510 BRANSON) and filtered using 0.45 µm nylon membrane filter. Then, the column was attached to the system and a pump was through the column. The flowrate and the pressure limit were set to 0.5 ml/min and 2.7 MPa, respectively. The sample was injected in the sample loop and run accordingly and was determined by calculating feed and permeate concentrations. The transmission of peptides can be defined as the ratio of solute concentration in the permeate (C_p) to feed concentration (C_f). MPH peptide transmission was calculated using equation (2) as described by (Roslan et al. 2017; Yunos & Field, 2008).

$$\text{Peptide transmission, } \Upsilon = \frac{C_p}{C_f} X\ 100 \quad (2)$$

KUMAR'S PORE-BLOCKING MODELS

Kumar's pore-blocking model was applied to analyze the fouling mechanisms in ultrafiltration of microalgae protein hydrolysate. In this study, the membrane configuration used for model fitting was the two-stage 10/5 kDa ultrafiltration system, as it exhibited the highest permeate flux among the tested configurations. The permeate obtained at the optimal fractionation conditions was analysed for fouling model fitting. The time (t) and volume of permeate (V) from MPH fractionation were used to calculate the linearized equations of cake formation, standard pore blocking and entire pore plugging model, which was adopted from Kumar's model (Md Zain & Mohammad, 2016). A graph of t/V (measured in min/L) versus V (measured in L) was created for the cake layer formation model, a graph of t/V (measured in min/L) versus t (measured in min) was plotted for the standard pore blocking model, and a graph of dV/dt (measured in L/min) versus V (measured in L) was generated for the complete pore plugging model. These graphs were created using different operating parameters, including flow rate, transmembrane pressure, and pH. The accuracy of Kumar's pore-blocking models have been assessed using the coefficient of determination (R^2) for statistical validation. The R^2 was calculated using equation (3) for each model and recorded .

$$R^2 = 1 - \frac{\sum(Jexp - Jmodel)^2}{\sum(Jexp - \bar{J}exp)^2} \quad (3)$$

CAKE LAYER FORMATION

The process of cake layer formation involves the formation of a layer on the surface of the membrane due to the accumulation of solute molecules that are larger than the pores of the membrane, preventing them from passing through. As the concentration of solute molecules is high, they accumulate on the membrane surface and in the previously deposited solute molecular layer, leading to the growth of a cake over time. This cake creates a porous barrier that increases the resistance of the membrane, reducing the flux. However, the cake can also enhance the removal efficiency of membrane particles. The characteristics of the cake formation model are described in equation (4). This is based on the research conducted by Vela et al. (2008) and Kumar et al. (2007).

$$\frac{t}{V} = \frac{1}{2}\left(\frac{\alpha\beta\mu}{\Delta PA^2}\right)V + \frac{\mu R_m}{\Delta PA} \quad (4)$$

where V is the permeate volume (m^3), α is the specific resistance of the cake that forms on the membrane surface (m/kg), β is the mass of particles per volume of filtrate (kg/m^3), ΔP is the transmembrane pressure (bar), A is the effective membrane surface (m^2), R_m is the membrane intrinsic resistance, µ is the viscosity of the feed water (Ns/m^2). The above equation can be expressed in terms of a linear relationship between the total permeate volume, V and the total filtration time, t as shown in equation (5).

$$\frac{t}{V} = X_1 V + Y_1 \quad (5)$$

STANDARD PORE-BLOCKING MODEL

The standard pore blocking model, also known as adsorptive fouling or pore narrowing, is characterized by the deposition of molecules on the pore walls of the membrane, leading to a reduction in the cross-sectional area of the pores and proportional decrease in the volume of the pores with the permeate volume. This model assumes that the fluid is Newtonian and that only pore narrowing occurs, with no complete pore blocking. This type of fouling is dominant when the retained molecules are smaller than the average pore size of the membrane and block the pores within the membrane. The standard pore

blocking model is described in equation (6), as outlined in the research conducted by Koonani and Amirinejad (2019), Vela et al. (2008), and Kumar et al. (2007).

$$\frac{t}{V} = t\left[\frac{\beta}{\pi L \rho_s}\left(\frac{\pi}{8\mu L}\right)^{1/2}\left(\frac{\mu R_m}{AN_p}\right)^{1/2}\right] + \frac{\mu R_m}{\Delta P A} \quad (6)$$

Where N_p is the number of open pores in the membrane and ρs is the density of the plugging particles (kg/m^3). A linear equation can be expressed in a simplified form as in equation (7).

$$\frac{t}{V} = tX_2 + Y_2 \quad (7)$$

COMPLETE PORE PLUGGING MODEL

The complete pore-plugging model describes the phenomenon where any molecule that reaches the surface of the membrane completely blocks the pores, and no molecule is deposited on top of another that has already settled on the surface. This results in a reduction in the available membrane area and an increase in membrane resistance, leading to a loss of filtering performance and the need for additional cleaning or replacement. In developing this model, several assumptions were made, including: (a) each particle contributes to the clogging process by closing one pore, and once the pore is closed, no other particles can enter or overlap with the particle, (b) there is no cake formation, and (c) the feed is Newtonian. Based on these assumptions, Kumar's model resulted in equation (8), which describes the complete pore-plugging model. This summary is based on the research conducted by Vela et al. (2008) and Kumar et al. (2007).

$$\frac{dV}{dt} = (N_{po} - p_p V)\frac{\pi \Delta P}{8\mu L} r_p^4 \quad (8)$$

where N_{po} is the total number of pores initially present, *Pp* is the number of plugging particles per volume of filtrate (m^{-3}), L is the length of pores (m) and r_p is the mean pore radius (m). From equation (8), the complete pore plugging model characteristic equation is also of linear form with a negative slope, it can be expressed in simplified form as equation (9). The intercept 'y' (dv/dt) of this equation indicates the permeate rate is a linear decreasing function of the volume filtered per unit time. Meanwhile, the negative slope indicates the decrease in the total number of pores that cause the fouling in complete pore plugging.

$$\frac{dV}{dt} = Y_3 - X_3 V \quad (9)$$

RESULTS & DISCUSSION

EFFECT OF FLOW RATE ON FLUX REDUCTION

Figure 3 demonstrates the effect of various flow rates on permeate flux for single stage 10 kDa and 5 kDa and two-stage 10/5 kDa. Interestingly, the 5 kDa membrane exhibits a higher flux than the 10 kDa membrane, which is contrary to conventional expectations. This behaviour can be attributed to differences in membrane structure, effective porosity, and fouling mechanisms. The 10 kDa membrane likely retains more large peptides, forming a dense fouling layer that restricts flux more than the 5 kDa membrane. Additionally, membrane pore compression at higher MWCO may contribute to reduced effective permeability. The observations indicate that the low flowrates result in higher permeate flux compared to higher flowrates. This is likely due to reduced concentration polarization (CP) and more stable diffusion layer at lower velocities, minimizing rapid pore blockage. as filtration progressed. Lower flow rates allow a more uniform concentration boundary layer to develop, reducing back diffusion resistance of peptides towards the membrane. On the contrary, at higher flowrates, increased turbulence may enhance fouling by accelerating particle deposition and internal pore blocking. This is because, at higher flow rates, shear stress increases, which might cause greater aggregation of peptides near the membrane surface, leading to faster fouling and a more significant flux decline. These observations align with previous studies on protein ultrafiltration, where flux behaviour is influenced by membrane properties, flow hydrodynamics and solute interactions (D'souza & Wiley 2016; Nur Sofuwani et al. 2016).

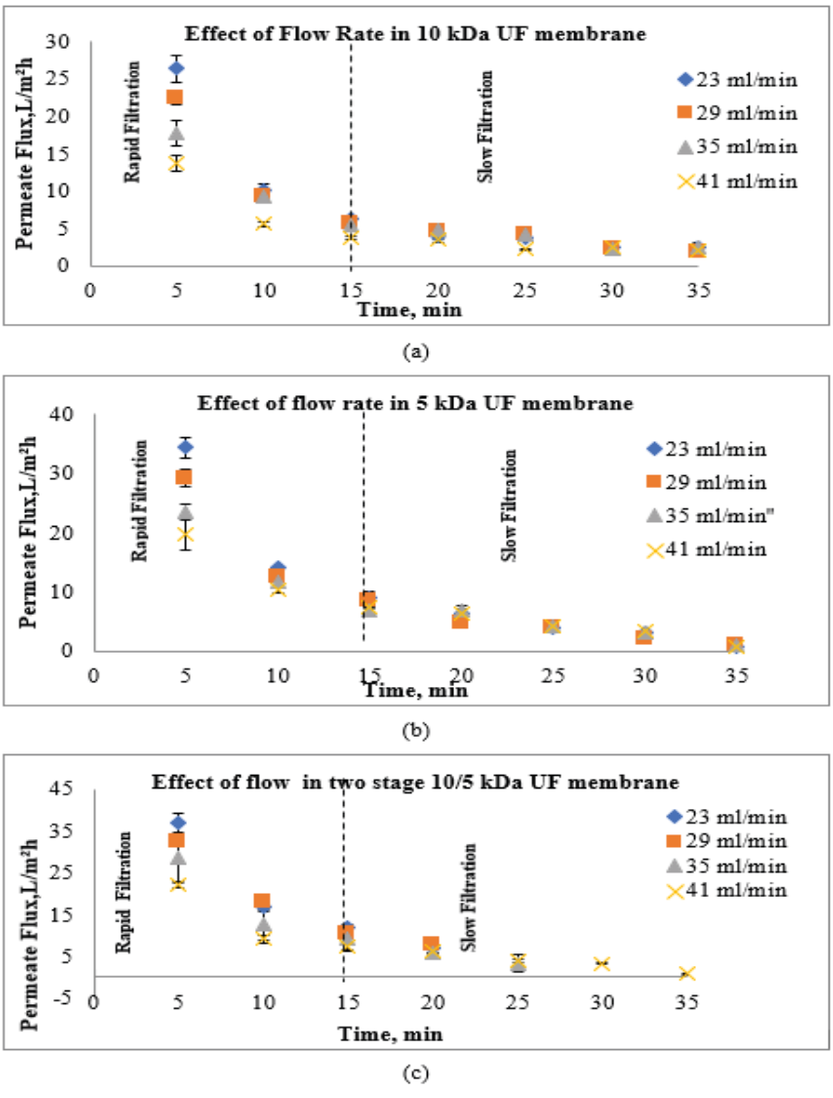

FIGURE 3. Effect of feed flow rate at constant TMP in (a) 10 kDa (b) 5 kDa (c) two-stage 10/5 kDa UF membrane (Fractionation at TMP of 0.5 Bar and pH 8)

EFFECT OF TRANSMEMBRANE PRESSURE ON FLUX REDUCTION

Three different TMPs (0.5, 1.0 and 1.5 Bar) with constant flow rates were chosen to investigate the influence of TMP on permeate flux and peptide transmission. Figure 4 (a) and (b) depict the permeate flow of MPH on a single membrane, while Figure 4 (c) depicts a two-stage 10/5 kDa membrane. The results indicate a gradual decline in permeate flux over time across all configurations, primarily due to fouling and concentration polarization (CP) effects. Although higher TMP initially increases flux by enhancing the driving force for filtration, excessive pressure accelerates fouling mechanisms, such as pore blocking and gel layer formation, ultimately restricting membrane permeability. This explains why flux at TMP 1.5 bar did not significantly outperform flux at 1.0 bar, as the rate of fouling exceeded the benefit of increased pressure. In a cross-flow hollow fiber membrane, the natural hydrodynamic pressure decreases from the inlet to the outlet as the mixed liquor (MPH) flows, leading to an uneven distribution of flux along the membrane. This uneven distribution results in concentration polarization, adding additional hydraulic resistance for the mixed liquor to flow through. Furthermore, concentration polarization within the membrane system contributed to flux decline. In cross-flow ultrafiltration, hydrodynamic pressure naturally decreases from the inlet to the outlet, creating an

uneven flux distribution along the membrane surface. This variation increases osmotic pressure, counteracting the applied TMP and further reducing the net driving force for filtration. As hydraulic resistance and osmotic pressure build up, the flow of microalgae protein hydrolysate (MPH) decreases, leading to a continuous decline in flux over time (Nur Sofuwani et al. 2016).

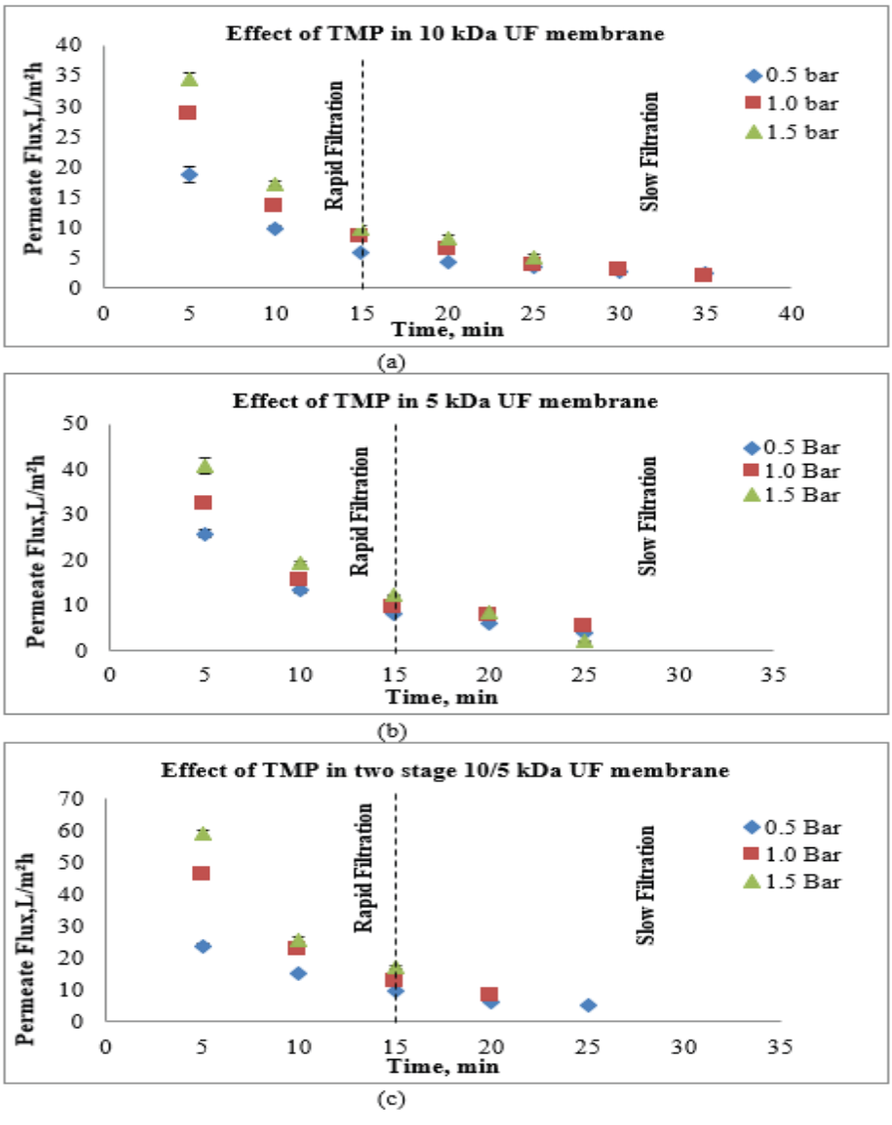

FIGURE 4. Effect of transmembrane pressure in (a) 10 kDa (b) 5 kDa (c) two-stage 10/5 kDa UF membrane (Fractionation at a flow rate of 23 ml/min and pH 8)

Interestingly, the 5 kDa membrane exhibited higher flux than the 10 kDa membrane, which can be attributed to differences in membrane structure and fouling behavior. The 10 kDa membrane retained larger peptides and protein aggregates, leading to a denser fouling layer that increased hydraulic resistance and restricted water passage. In contrast, the 5 kDa membrane allowed more uniform solute retention, preventing rapid pore clogging and maintaining a higher effective flux. In a 10 kDa membrane, filtration initially proceeded rapidly before gradually slowing down until completion. At 25 minutes of filtering, the permeate flow for three different TMP levels began to intersect and peak, suggesting that any further increase in TMP did not affect the flow, indicating that the permeate had reached its limiting flux. This phenomenon may be attributed to concentration polarization and membrane fouling (Wu et al. 1999). Below 25 minutes of filtration, a critical flux can effectively mitigate fouling phenomena. Besides, in the 5 kDa membrane, rapid filtration was observed in the first 15 minutes, with permeate flux at TMP levels of 0.5 and 1.0 Bar reaching a plateau, indicating that these TMP levels

reached the limiting flux at 15 minutes. However, at TMP 1.5 Bar, the permeate flux overlapped with TMP 1.0 Bar and continued to decrease until reaching 1.9714±0.0857 L/m^{2}h. At higher TMP, reduced hydraulic resistance allowed the UF membrane to filter more MPH, thus not limiting the permeate flux. Permeate flux for all TMP levels using the 5 kDa membrane ceased at 25 minutes due to increased osmotic pressure counteracting the feed flow. Similarly, in two-stage 10/5 kDa membrane, rapid filtration occurred in the first 15 minutes, but the filtration process stopped earlier. Less time was required for filtration as TMP increased, with the process halting at 15, 20 and 25 minutes for TMP levels of 1.5, 1.0 and 0.5 Bar, respectively. During the second stage of filtration, the removal of larger molecules than 10 kDa at the first stage led to a reduction in feed viscosity. Lower viscosity facilitated a greater mass transfer process through the membrane, reducing hydraulic resistance and accelerating the filtration process especially at high TMP levels (Zuhair et al. 2018).

EFFECT OF PH ON FLUX REDUCTION

pH played a significant role in ultrafiltration (UF) by altering the chemical composition, charge interactions and aggregation behaviour of the microalgae protein hydrolysate (MPH). In this study, pH levels ranging from acidic to alkaline conditions (pH 2, 4, 7, 9 and 11) were examined at a constant flow rate of 23 ml/min and TMP of 0.5 Bar to examine their impact on MPH separation. Fig. 5 (a) and (b) presents the permeate flux against time at different pH levels using single membranes of 10 and 5 kDa, respectively, while Fig. 5 (c) shows the permeate flux using two-stage membrane 10/5 kDa. For the 10 kDa membranes, a rapid increase in flux was observed for the first 20 minutes, followed by stabilization phase. Within the first 5 minutes, the highest flux was recorded at pH 9, followed by pH 7, 11, 4 and 2. After 15 minutes, the flux values for pH 2, 4, 7 and 11 overlapped and remained constant until the end of filtration. A similar trend was observed for the 5kDa membrane, suggesting that membrane pore size had minimal influence on pH-driven flux variations.

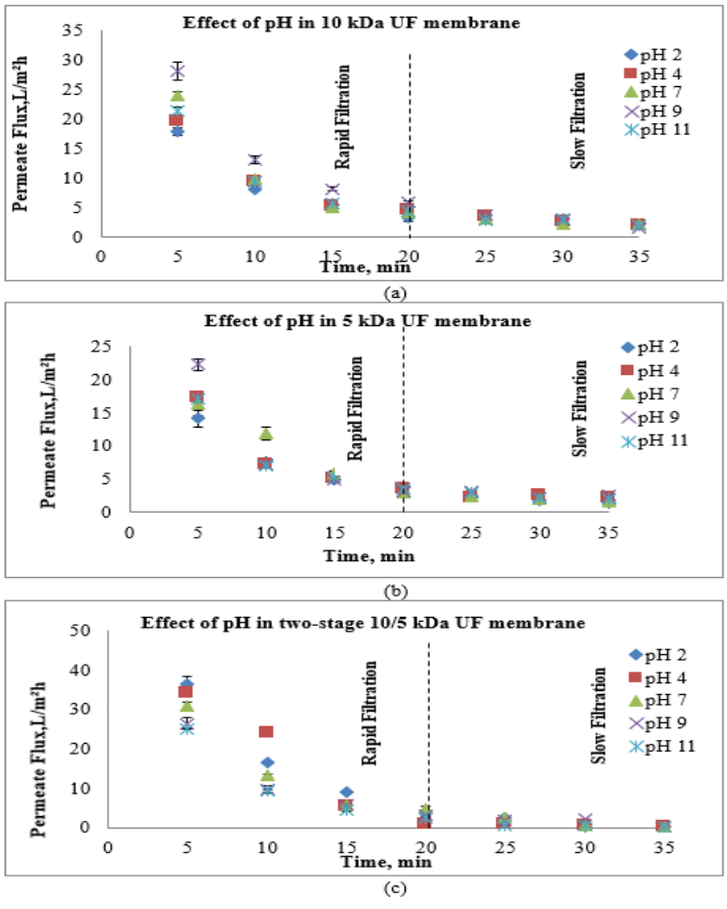

FIGURE 5. Effect of pH in (a) 10 kDa (b) 5 kDa (c) two-stage 10/5 kDa UF membrane (Fractionation at flow rate of 23 ml/min and TMP of 0.5 Bar)

The differences in permeate flux at various pH levels were primarily attributed to protein solubility and minimal aggregation, resulting in a lower viscosity solution and thus higher permeate flux (Wang et al, 2019). In contrast, at pH 2, proteins approached their isoelectric point (pI), leading to extensive aggregation and gel layer formation, which significantly reduced flux (Miller et al 2020). Interestingly, the two-stage 10/5 kDa membrane system exhibited a different trend, where pH 2 resulted in the highest flux during the first 5 minutes, followed by pH 4, 7, 9, and 11. This suggests that in a two-stage filtration system, acidic conditions may enhance initial membrane permeability by modifying protein-protein interactions in a way that reduces rapid membrane fouling. Similar findings have been reported in protein fractionation studies, where controlled acidic environments can improve initial flux performance due to modified electrostatic interactions between peptides and the membrane surface (Liu et al. 2021). These findings highlight the importance of pH in optimizing ultrafiltration performance, as it directly influences protein solubility, aggregation, and fouling tendencies. The observed differences between single and two-stage membrane systems suggest that adjusting pH conditions could be a key strategy to enhance peptide fractionation efficiency while minimizing membrane fouling.

EFFECT OF DIFFERENT MEMBRANE PORE SIZES AND CONFIGURATION ON PERMEATE FLUX

The effectiveness of membrane operations for MPH can be evaluated based on the permeate flux and peptide transmission. The results indicate membrane pore sizes significantly influence both parameters, where the 10 kDa membrane exhibited lower permeate flux and peptide transmission compared to a 5 kDa membrane under identical operating conditions. This behaviour contradicts the general expectation that larger membrane pore sizes often experience more severe fouling, leading to lower effective permeability (Gerardo et al. 2014; Hwang et al. 2008; Siddiqui et al. 2016). Hwang et al. (2008) reported that 0.4 µm membranes had a higher blocking index than 0.2 µm membrane, indicating greater susceptibility to membrane fouling despite the larger pore size. This phenomenon occurs because larger pores allow greater penetration of foulants into membrane structure, leading to internal pore blockage and increased hydraulic resistence. Once the pores blocked, filtration transitions into cake layer formation, further reducing flux and separation efficiency (Hughes & Field, 2006).

The membrane configuration, in addition to its pore size, plays a significant role in achieving the desired permeate flux. This study compared two membrane configurations, single-stage and two-stage membranes, and found the two-stage system (10/5 kDa) exhibited superior performance in terms of both permeate flux and peptide transmission. One possible explanation for this could be the change in viscosity of the mixed permeate (MPH) during the filtration process using a two-stage membrane (Zuhair et al. 2018). In the first stage of filtration, a

10 kDa membrane retains most macromolecules larger than 10 kDa, resulting in a less viscous permeate that is further filtered in the second stage using a 5 kDa membrane. This reduction in viscosity can decrease the fouling effect in the membrane and enhance the performance of the ultrafiltration membrane. Table 1 summarizes the membrane filtration for MPH using different membrane pore sizes and configurations. The optimal operating parameters were selected based on the highest permeate flux and peptide transmission efficiency. Given the influence of flow rate, transmembrane pressure (TMP) and pH on membrane performance, these factors should be considered in tandem with pore size and configuration to optimize separation efficiency and minimize fouling effects.

TABLE 1. The best operating parameters for different membrane pore sizes and configurations

Membrane pore size (kDa)	Configuration membrane	Parameters			Total permeate flux (L/m²h)	Total Peptide Transmission (%)
		Flow Rate (ml/min)	TMP (Bar)	pH		
10	Single	23	1.5	9	43.65±1.10	58.20±0.66
5	Single	23	1.5	9	55.42±0.50	67.34±0.83
10/5	Two-stage	23	1.5	2	69.85±1.22	79.13±0.50

FOULING ANALYSIS

The permeate flux patterns revealed a decline in UF membrane performance over time, with variations observed under different operating conditions. Fouling emerged as the primary cause flux reduction, leading to decreased peptide transmission. Therefore, understanding fouling mechanisms is essential to optimize ultrafiltration conditions and mitigate performance deterioration. Based on the highest permeate flux obtained, a two-stage 10/5 kDa ultrafiltration membrane configuration was selected to investigate fouling behavior under various operating parameters. Three pore-blocking models (cake formation, standard pore blocking and complete pore plugging) were applied to the data to analyze fouling effects.

TABLE 2. The value of R^2 obtained from the experimental data in the study of the effect of pH on membrane fouling

Configuration membrane	pH	R^2		
		Cake Formation Model	Standard Pore Blocking Model	Complete Pore Plugging Model
Two-stage 10/5 kDa	2	0.629	0.9386	0.7832
	4	0.3765	0.9171	0.3803
	7	0.7838	0.9549	0.8861
	9	0.9289	0.9906	0.984
	11	0.7542	0.9813	0.9165

Given that the peptides filtered in the second step were smaller than 10 kDa, it was anticipated that filtration would primarily follow standard pore-blocking and complete pore-plugging models. Furthermore, as discusses earlier, pH significantly influences peptide conformation and solubility, making it crucial factor in fouling behaviour. The results indicated that the standard pore-blocking model provided the fit for ultrafiltration of MPH across different pH levels, suggesting that peptides smaller than 5 kDa penetrated membrane pores and adhered to the inner pore surface, leading to accumulation and an increase in concentration polarization, and exacerbated fouling. Table 2 shows that the highest R^2 values were observed at pH 9 (R^2=0.9906) and pH 11 (R^2=0.9813), indicating significant fouling in alkaline conditions. This finding aligns with the observed decline in permeate flux at high pH, likely due to reduced electrostatic repulsion between peptides and the PES hollow fiber membrane, which promotes peptide aggregation and membrane blockage. In contrast, at low pH (pH 2), the higher surface charge and stronger electrostatic repulsion between peptides and membrane facilitated greater peptide back diffusion to the feed side, resulting in lower peptide accumulation, reduced fouling and higher flux. Therefore, the standard pore-blocking model exhibited lower R^2 values in acidic regions, reflecting reduced fouling intensity.

In addition to solution pH, transmembrane pressure (TMP) significantly influenced fouling in UF membranes. TMP impacts both reversible and irreversible filtration resistance, with higher pressures leading to increased solute accumulation near the membrane surface, promoting irreversible adsorption and membrane fouling (Briao & Tavares, 2012). Pore-blocking model equations were used to analyze experimental permeate flow data at various TMP levels (Table 3). The results showed that standard pore blocking was the dominant fouling mechanism at various TMP levels, similar to the impact of pH. The lowest R^2 (0.8908) was observed at TMP 0.5 Bar, while the highest R^2 value was obtained at TMP 1.0 Bar, indicating increased fouling at this pressure range. These findings aligns with those of Briao & Tavares (2012), who reported that although high TMP initially increases permeate flux, it is also enhances total filtration resistance, leading to membrane fouling. Additionally, Vela et al. (2008) observed that fouling is less severe at lower TMP, as flux is governed by Darcy's Law, whereas at higher TMP, flux becomes independent of pressure due to concentration polarization. The small difference in R^2 values (less than 4%) across three pore-blocking models suggests that cake formation, standard pore blocking and complete pore plugging models may occur simultaneously, depending on solute and membrane conditions.

The value of R^2 obtained from the experimental data in the study of the effect of trans-membrane pressure on membrane fouling Feed flow rate was another critical factor affecting membrane fouling. Table 4 presents the R^2 values obtained during experiments, showing that the standard pore-blocking model was the best fit for most flow rates, except a flow rate of 29 ml/min, where a cake forming model was suggested. The highest R^2 (0.6299) was observed at a flow rate of 23 ml/min, indicating increased fouling at a lower flow rate. Experiments were conducted at a constant TMP of 1.5 Bar, and results revealed that high TMP combined with low flow rates led to the accumulation of solute molecules on the membrane surface, promoting fouling (Vela et al. 2008). Notably, most R^2 values in Table 4 were below 0.9, indicating imperfect model fits, suggesting that a combination of pore-blocking model mechanisms occurs simultaneously. Moreover, comparing R^2 values across different flow rates did not consistently indicate a better model fit. Vela et al, (2008) suggested that comparing R^2 values across different pore-blocking models under the same experimental conditions provide more meaningful insights than comparing vmodels under varying conditions despite the higher probability of fouling at a flow rate of 23 ml/min, this condition demonstrated good membrane performance in terms of permeate flux, due to challenges in measuring flux accurately during the early stages of ultrafiltration experiments.

TABLE 3. The value of R^2 obtained from the experimental data in the study of the effect of trans-membrane pressure on membrane fouling

Configuration membrane	TMP, Bar	R^2		
		Cake Formation Model	Standard Pore Blocking Model	Complete Pore Plugging Model
Two-stage 10/5 kDa	0.5	0.8691	0.8908	0.8731
	1	0.9158	0.9522	0.9337
	1.5	0.9282	0.9286	0.9186

In summary, pore blocking models (cake development, standard pore blocking, and total pore plugging) provide insight into fouling mechanisms under various membrane operating conditions, including pH solution, transmembrane pressure, and feed flow rate. These parameters, along with fouling behaviour, influenced concentration polarization effects, which further contributed to flux decline. The nature and extent of fouling depended on solute-membrane interactions, where solute size relative to membrane pore diameter determined the dominant pore-blocking mechanism. When solute size exceeded pore size, fouling followed total pore plugging, progressing to standard pre blocking as particles accumulated, eventually resulting in cake formation. Therefore, multiple fouling mechanisms may occur simultaneously at different stages, reinforcing the complexity of fouling in MPH filtration processes.

TABLE 4. The value of R^2 obtained from the experimental data in the study of the effect of flow rate on membrane fouling

Configuration membrane	Flow Rate, ml/min	R^2		
		Cake Formation Model	Standard Pore Blocking Model	Complete Pore Plugging Model
Two-stage 10/5 kDa	23	0.5766	0.6299	0.578
	29	0.2029	0.1731	0.1838
	35	0.5283	0.6282	0.55
	41	0.1317	0.2204	0.123

CONCLUSION

The flux reductions for all parameters reached a steady state within 20 to 35 minutes. The trends of flux reduction behavior for microalgae protein hydrolysate were consistent across different operating parameters, including transmembrane pressure (TMP), stirring speed and pH. The highest permeate fluxes for single-membrane filtration was observed at pH 9, 1.5 bar, and a flow rate of 23 ml/min, with values of 43.65±1.10 L/m^2h for the 10 kDa membrane and 55.42±0.50 L/m^2h for the 5 kDa membrane. Meanwhile, the two-stage 10/5 kDa membrane configuration exhibited the highest permeate flux (69.85±1.22 L/m^2h) at pH 2, 1.5 bar and at a flow rate of 23 ml/min, indicating enhanced separation efficiency under acidic conditions.

In addition to permeate flux, peptide transmission was significantly influenced by membrane configuratib and

oerating conditions. The two-stage membrane system demonstrated superior peptide transmission efficiency, with a higher proportion of low-molecular weight peptides (<5 kDa) successfully passing through the membrane compared to single-membrane filtration. This highlights the effectiveness of staged fractionation in optimizing peptide recovery.

The best experimental setup for fractionation of microalgae protein hydrolysate *Nannochloropsis sp* was achieved using a two-stage 10/5 kDa configuration, which further evaluated for its fouling behaviour using Kumar's model. The standard pore-blocking model provided the best fit across all operating conditions, confirming that smaller peptides penetrated membrane pores, leading to gradual flux reduction due to internal pore adsorption. Controlling flow rate, transmembrane pressure and pH effectively minimized fouling and concentration polarization, ensuring higher permeate flux and improved peptide transmission. The findings from this study provide a deeper understanding of the ultrafiltratoion-based fractionation of microalgae protein hydrolysates and demonstrate the potential for obtaining high yield of functional peptides. This research contributes valuable insights for optimizing membrane separation in bioactive peptide recovery.

ACKNOWLEDGEMENT

The authors thank to Universiti Putra Malaysia for funded this project : geran PUTRA, GP-IPS/2019/9635800

DECLARATION OF COMPETING INTEREST

None.

REFERENCES

Abidin, A.A.Z., Suntarajh, M. & Yusof, Z.N.B. 2020. Transformation of a Malaysian species of *Nannochloropsis*: Gateway to construction of transgenic microalgae as vaccine delivery system to aquatic organisms. *Bioengineered* 11(1): 1071–1079.

Agrawal, H., Joshi, R. & Gupta, M. 2017. Isolation and characterisation of enzymatic hydrolysed peptides with antioxidant activities from green tender sorghum. *LWT – Food Science and Technology* 84: 608–616.

Aluko, R.E. & Nwachukwu, I.D. 2018. Antioxidant properties of flaxseed protein hydrolysates: Influence of hydrolytic enzyme concentration and peptide size. *Journal of the American Oil Chemists' Society*: 1–14.

Bazinet, L. & Firdaous, L. 2009. Membrane processes and devices for separation of bioactive peptides. *Recent Patents on Biotechnology* 3: 61–72.

Briao, V. & Tavares, C.R.G. 2012. Pore blocking mechanism for the recovery of milk solids from dairy wastewater by ultrafiltration. *Brazilian Journal of Chemical Engineering* 29(2): 393–407.

Chen, L., Liu, J., Gao, X. et al. 2021. Optimizing transmembrane pressure for protein ultrafiltration. *Separation Science and Technology* 56(2): 198–210.

Cheryan, M. & Mehaia, M. 1986. Membrane bioreactors. Dlm. Gregor, M. (pnyt.). *Membrane Separation in Biotechnology*: 255–301. New York: Marcel Dekker, Inc.

D'Souza, N. & Wiley, D.E. 2016. Whey ultrafiltration: Effect of operating parameters on flux and rejection. Dlm. *Proceedings of the 5th International Membrane Science and Technology Conference*: 1–6.

Fan, J., He, J., Zhuang, Y. & Sun, L. 2012. Purification and identification of antioxidant peptides from enzymatic hydrolysates of tilapia (*Oreochromis niloticus*) frame protein. *Molecules* 17: 12836–12850.

Field, R.W., Wu, D., Howell, J.A. & Gupta, B.B. 1995. Critical flux concept for microfiltration fouling. *Journal of Membrane Science* 100: 259–272.

Fouzia, Y., Abdelouahab, N., Amal, K. & Slimane, B. 2015. Whey ultrafiltration: Effect of pH on permeate flux and proteins retention. *World Applied Sciences Journal* 33(5): 744–751.

Gerardo, M.L., Oatley-Radcliffe, D.L. & Lovitt, R.W. 2014. Integration of membrane technology in microalgae biorefineries. *Journal of Membrane Science* 464: 86–99.

Gouveia, L. & Oliveira, A.C. 2009. Microalgae as a raw material for biofuels production. *Journal of Industrial Microbiology & Biotechnology* 36: 269–274.

Ho, C. & Zydney, A. 2000. A combined pore blockage and cake filtration model for protein fouling during microfiltration. *Journal of Colloid and Interface Science* 232: 389–399.

Hughes, D. & Field, R.W. 2006. Crossflow filtration of washed and unwashed yeast suspensions at constant shear under nominally sub-critical conditions. *Journal of Membrane Science* 280: 89–98.

Hwang, K., Liao, C. & Tung, K. 2008. Effect of membrane pore size on the particle fouling in membrane filtration. *Desalination* 234: 16–23.

Koonani, H. & Amirinejad, M. 2019. Combined three mechanisms models for membrane fouling during microfiltration. *Journal of Membrane Science & Research* 5: 274–282.

Kumar, S.M., Madhu, G.M. & Roy, S. 2007. Fouling behaviour, regeneration options and on-line control of biomass-based power plant effluents using microporous ceramic membranes. *Separation and Purification Technology* 57: 25–36.

Liu, F., Ma, Y., Zhao, X. et al. 2020. Effect of operational parameters on protein ultrafiltration performance. *Separation and Purification Technology* 239: 116536.

Liu, F., Ma, Y., Zhao, X. et al. 2021. Effect of pH on membrane performance in protein ultrafiltration: A mechanistic study. *Separation and Purification Technology* 275: 119091.

Md Zain, M. & Mohammad, A.W. 2016. Effect of pH on flux decline during fractionation of glucose from cellulose hydrolysate through a polysulfone membrane. *Malaysian Journal of Analytical Science* 20(6): 1413–1420.

Medina, C., Rubilar, M., Shene, C., Torres, S. & Verdugo, M. 2015. Protein fractions with techno-functional and antioxidant properties from *Nannochloropsis gaditana* microalgal biomass. *Journal of Biobased Materials and Bioenergy* 9: 1–9.

Miller, D.J., Kasemset, S., Paul, D.R. et al. 2020. Influence of protein solubility and aggregation on membrane fouling. *Journal of Membrane Science* 604: 118018.

Nguyen, M.H.T., Qian, Z., Nguyen, V., Choi, I., Heo, S., Oh, C.H. et al. 2013. Tetrameric peptide purified from hydrolysates of biodiesel byproducts of *Nannochloropsis oculata* induces osteoblastic differentiation through MAPK and Smad pathway on MG-63 and D1 cells. *Process Biochemistry* 48: 1387–1394.

Nur Sofuwani, Z.A., Siti Aslina, H. & Siti Mazlina, M. 2016. Separation of lactose from raw goat's milk by cross-flow hollow fiber ultrafiltration membrane. *International Food Research Journal* 23: 209–219.

Quezada, C., Estay, H., Cassano, A., Troncoso, E. & Ruby-Figueroa, C. 2021. Prediction of permeate flux in ultrafiltration processes: A review of modeling approaches. *Membranes* 11(368): 1–37.

Roslan, J., Mazlina, S., Kamal, M., Faezah, K. & Abdullah, N. 2017. Assessment on multilayer ultrafiltration membrane for fractionation of tilapia by-product protein hydrolysate with angiotensin I-converting enzyme (ACE) inhibitory activity. *Separation and Purification Technology* 173: 250–257.

Samarakoon, K.W., O-Nam, K., Ko, J., Lee, J.-H., Kang, M.-C., Kim, D. et al. 2013. Purification and identification of novel angiotensin-I converting enzyme (ACE) inhibitory peptides from cultured marine microalgae (*Nannochloropsis oculata*) protein hydrolysate. *Journal of Applied Phycology* 25: 1595–1606.

Siddiqui, M.U., Arif, A.F.M. & Bashmal, S. 2016. Permeability–selectivity analysis of microfiltration and ultrafiltration membranes: Effect of pore size and shape distribution and membrane stretching. *Membranes* 6(40): 1–14.

Singh, N. & Cheryan, M. 1998. Membrane technology in corn refining and bioproduct processing. *Starch* 50: 16–23.

Vela, M.C.V., Blanco, S.A., Garcia, J.L. & Rodriduez, E.B. 2008. Analysis of membrane pore blocking models applied to the ultrafiltration of PEG. *Separation and Purification Technology* 62: 489–498.

Wang, Y. & Tang, C.Y. 2011. Fouling of nanofiltration, reverse osmosis, and ultrafiltration membranes by protein mixtures: The role of inter-foulant-species interaction. *Environmental Science and Technology* 45: 6373–6379.

Wang, X., Zhang, L., Wu, H. et al. 2019. pH-dependent fouling mechanisms in protein ultrafiltration. *Membrane Science Journal* 48(3): 285–296.

Wu, D., Howell, J. & Field, R. 1999. Critical flux measurement for model colloids. *Journal of Membrane Science* 152: 89–98.

Zain, M.M., Mohammad, A.W. & Hairom, N.H.H. 2017. Flux and permeation behaviour of ultrafiltration in sugaring out cellulose hydrolysate solution: A membrane screening. *Journal of Physical Science* 28: 25–38.

Zuhair, M., Nor, M. & Vasiljevic, T. 2018. Performance of a two-stage membrane system for bromelain separation from pineapple waste mixture as impacted by enzymatic pretreatment and diafiltration. *Food Technology and Biotechnology* 56(2): 218–227.

Callister, W.D. 2000. *Materials Science and Engineering: An Introduction.* 5th ed. New York: John Wiley & Sons.

Zainol, M.M., Amin, N.A.S. & Asmadi, M. 2017. Preparation and characterization of impregnated magnetic particles on oil palm frond activated carbon for metal ions removal. *Sains Malaysiana* 46(2): 773–782.